INT. J. REMOTE SENSING, 2001, VOL. 22, NO. 18, 3719–3746

A mono-window algorithm for retrieving land surface temperature from Landsat TM data and its application to the Israel-Egypt border region

Z. QIN*, A. KARNIELI†

The Remote Sensing Laboratory, Department of Environmental Physics, J. Blaustein Institute for Desert Research, Ben Gurion University of the Negev, Sede Boker Campus, 84990, Israel

and P. BERLINER

The Wyler Laboratory for Arid Land Conservation and Development, Department of Dryland Agriculture, J. Blaustein Institute for Desert Research, Ben Gurion University of the Negev, Sede Boker Campus, 84990, Israel

(*Received 28 September 1999; in final form 9 June 2000*)

Abstract. Remote sensing of land surface temperature (LST) from the thermal band data of Landsat Thematic Mapper (TM) still remains unused in comparison with the extensive studies of its visible and near-infrared (NIR) bands for various applications. The brightness temperature can be computed from the digital number (DN) of TM6 data using the equation provided by the National Aeronautics and Space Administration (NASA). However, a proper algorithm for retrieving LST from the only one thermal band of the sensor still remains unavailable due to many difficulties in the atmospheric correction. Based on thermal radiance transfer equation, an attempt has been made in the paper to develop a mono-window algorithm for retrieving LST from Landsat TM6 data. Three parameters are required for the algorithm: emissivity, transmittance and effective mean atmospheric temperature. Method about determination of atmospheric transmittance is given in the paper through the simulation of atmospheric conditions with LOWTRAN 7 program. A practicable approach of estimating effective mean atmospheric temperature from local meteorological observation is also proposed in the paper when the *in situ* atmospheric profile data is unavailable at the satellite pass, which is generally the case in the real world especially for the images in the past. Sensitivity analysis of the algorithm indicates that the possible error of ground emissivity, which is difficult to estimate, has relatively insignificant impact on the probable LST estimation error δT, which is sensible to the possible error of transmittance $\delta\tau_6$ and mean atmospheric temperature δT_a. Validation of the simulated data for various situations of seven typical atmospheres indicates that the algorithm is able to provide an accurate LST retrieval from TM6 data. The LST difference between the retrieved and the simulated ones is less than 0.4°C for most situations. Application of the algorithm to the sand dunes across the Israel–Egypt border results in a reasonable LST

*Current address of Z. Qin is SMC, the Spatial Modelling Center, Box 839, S-981 28 Kiruna, Sweden; e-mail: qin.zhihao@smc.kiruna.se

†e-mail: karnieli@bgumail.bgu.ac.il

International Journal of Remote Sensing
ISSN 0143-1161 print/ISSN 1366-5901 online © 2001 Taylor & Francis Ltd
http://www.tandf.co.uk/journals
DOI: 10.1080/01431160010006971

estimation of the region. Based on this LST estimation, spatial variation of the interesting thermal phenomenon has been analysed for comparison of LST difference across the border. The result shows that the Israeli side does have significantly higher surface temperature in spite of its denser vegetation cover than the Egyptian side where bare sand is prevalent.

1. Introduction

The Landsat Thematic Mapper (TM) images have been extensively studied for various purposes (Kaneko and Hino 1996, Lo 1997, Caselles *et al.* 1998). Searching with the keyword Landsat TM on the world-widely used CD-ROM scientific abstract database GEOBASE for the period 1980–1999 pops out 1043 papers written in English. Except the six bands in visible and near- infrared (NIR) wavelengths, the remote sensor also has a thermal band (TM6) operating in the wavelength range of 10.45–12.50 μm with a nominal ground resolution of 120 m $\times$ 120 m. This spatial resolution of Landsat TM6 is high enough for analysing the detailed spatial patterns of thermal variation on the Earth's surface. However, when searching on the GEOBASE with the restricted keyword temperature, only 73 papers were found. Detailed examination of these papers reveals that only 35 of them relating to the surface temperature or thermal band data of Landsat TM. This implies that the study of Landsat TM thermal band for surface temperature and its application still remains as an ignored area. This is especially true when referring to land surface temperature (LST). Due to its high spatial resolution, Landsat TM6 has considerable potential for many applications relating to LST. Some studies relating to the thermal band of Landsat TM only use the brightness temperature at the satellite level (Mansor *et al.* 1994, Saraf *et al.* 1995, Zhang *et al.* 1997) or just simply use the digital number (DN) value for their applications (Ritchie *et al.* 1990, Oppenheimer 1997). The actual use of LST retrieved from Landsat TM6 is few (Hurtado *et al.* 1996, Sospedra *et al.* 1998). In addition to its intrinsic weaknesses (no on-board calibration, low repeat frequency, and so on), the lack of a proper and easily-used algorithm for retrieval of LST from the only one thermal band of Landsat TM data probably is also the main reason leading to the few application.

Up to present, the studies of Landsat TM thermal data mainly concentrate on the level of directly applying brightness temperature or DN value to the issues in the real world and on the study of the sea/lake surface temperature corrected with atmospheric model using radiosonde data. Zhang *et al.* (1997), Saraf *et al.* (1995) and Mansor *et al.* (1994) demonstrated that the radiant temperature converting from Landsat TM thermal data is capable of application for detection of subsurface coal fires. Sugita and Brutsaert (1993) compared the measured LST in the field with the temperature from satellite including Landsat TM. The measured sea surface temperature is found to be about 7.8°C higher than the brightness temperature for Landsat TM6 around the outlet of a nuclear power plant (Liu and Kuo 1994). Haakstad *et al.* (1994) demonstrated the importance of Landsat TM6 data in sea temperature study for identifying the surface current patterns. Relationship between water quality indicators and Landsat TM digital data including TM6 DN value has been analysed in the study of Braga *et al.* (1993) about water quality assessment at Guanabara Bay of Brazil. Oppenheimer (1997) used the relationship between the measured lake surface temperature and Landsat TM6 DN value to map the thermal variation of volcano lakes. Correlation of lake suspended sediments with digital data of Landsat MSS and TM was analysed in Ritchie *et al.* (1990). Based on the surface temperature

derived from Landsat TM thermal data, Moran *et al.* (1989) estimated the latent heat and net radiant flux density and compared with the ground estimate based on Bowen ratio measurement over mature fields of cotton, wheat and alfalfa. The Landsat TM6 data has been used in several studies to investigate the thermal properties of volcanoes (Reddy *et al.* 1990, Andres and Rose 1995, Kaneko 1998).

Provided that ground emissivity is known (the determination of emissivity is very complicated and there is a great volume of literature on it), the retrieval of LST from Landsat TM6 is mainly through the method of atmospheric correction. The principle of the correction is to subtract the upward atmospheric thermal radiance and the reflected atmospheric radiance from the observed radiance at satellite level so that the brightness temperature at ground level can be directly computed. The atmospheric thermal radiance can be simulated using such atmospheric simulation programs as LOWTRAN, MODTRAN or 6S when *in situ* atmospheric profile is available at the satellite pass. Usually this is not the case for many applications. Thus, an alternative is to use the available radiosonde data closed to the satellite pass or with similar atmospheric conditions for this atmospheric simulation (Hurtado *et al.* 1996). In many cases, even the radiosonde data is also not available due to difficulties for the measuring. This unavailability of *in situ* atmospheric profile data prevents the popular application of LST retrieval from Landsat TM6 for many studies. Alternately, the standard atmospheric profiles provided in the atmospheric simulation programs were used to simulate the atmospheric radiance for retrieval of surface temperature from the Landsat TM thermal data.

An attempt was made by Hurtado *et al.* (1996) to compare the two atmospheric correction methods for Landsat TM thermal band. Using surface energy balance equation and standard meteorological parameters, they proposed a method of atmospheric correction for Landsat TM thermal data. Alternately, the required parameters for atmospheric correction were calculated from a radiative transfer model using the atmospheric profiles obtained from local temporarily coincident radiosondes. The latter atmospheric correction method has been on the right way of developing an algorithm for LST retrieval from Landsat TM6 data but it involves several parameters that are not easy to estimate for most cases. This is the only study published to attempt an algorithm development for LST retrieval from one thermal band data.

Based on the thermal radiance transfer equation, the current study attempts to develop an algorithm for retrieving LST from Landsat TM6 data. Because this algorithm is suitable for LST retrieval from only one thermal band data, it has been termed as the mono-window algorithm in order to distinguish from split window algorithm for two thermal channels. Compared to the several atmospheric parameters required in the second correction method of Hurtado *et al.* (1996), the mono-window algorithm only requires two atmospheric parameters (transmittance and mean atmospheric temperature) for LST retrieval. Moreover, the detailed estimation of these two critical atmospheric parameters is also addressed for practical purpose of applying the algorithm. Then, we perform the sensitivity analysis of the algorithm for the critical parameters and validate it to the simulated data for various situations of seven typical atmospheres. Finally, we try to present an example of its application to the sand dunes across the Israel–Egypt political border for examination of the LST difference on both sides of the border region.

2. Computing brightness temperature of Landsat TM6 data

The development of the mono-window algorithm for LST retrieval from the thermal band data of Landsat TM is with premise that the brightness temperature

of the thermal band at the satellite level can be computed from the data. Generally, the grey level of Landsat TM data is given as digital number (DN) ranging from 0 to 255. Thus, the computation of brightness temperature from TM6 data includes the estimation of radiance from its DN value and the conversion of the radiance into brightness temperature.

The following equation developed by the National Aeronautics and Space Administration (NASA) (Markham and Barker 1986) is generally used to compute the spectral radiance from DN value of TM data:

$$L_{(\lambda)} = L_{\min(\lambda)} + (L_{\max(\lambda)} - L_{\min(\lambda)})Q_{\mathrm{dn}}/Q_{\max} \tag{1}$$

where $L_{(\lambda)}$ is the spectral radiance received by the sensor (mW cm^{-2} sr^{-1} μm^{-1}), $Q_{\max}$ is the maximum DN value with $Q_{\max} = 255$, and Q_{dn} is the grey level for the analysed pixel of TM image, $L_{\min(\lambda)}$ and $L_{\max(\lambda)}$ are the minimum and maximum detected spectral radiance for $Q_{\mathrm{dn}} = 0$ and $Q_{\mathrm{dn}} = 255$, respectively. For TM6 of Landsat 5 with central wavelength of 11.475 μm, it has been set that $L_{\min(\lambda)} = 0.1238$ for $Q_{\mathrm{dn}} = 0$ and $L_{\max(\lambda)} = 1.56$ mW cm^{-2} sr^{-1} μm^{-1} for $Q_{\mathrm{dn}} = 255$ (Schneider and Mauser 1996). Thus, the above equation can be simplified into the following form:

$$L_{(\lambda)} = 0.1238 + 0.005632156Q_{\mathrm{dn}} \tag{2}$$

Once the spectral radiance $L_{(\lambda)}$ is computed, the brightness temperature at the satellite level can be directly calculated by either inverting Planck's radiance function for temperature (Sospedra *et al.* 1998) or using the following approximation formula (Schott and Volchok 1985, Wukelic *et al.* 1989, Goetz *et al.* 1995):

$$T_6 = K_2/\ln(1 + K_1/L_{(\lambda)}) \tag{3}$$

where T_6 is the effective at-satellite brightness temperature of TM6 in K, K_1 and K_2 are pre-launch calibration constants. For Landsat 5, which we will use in the study, $K_1 = 60.776$ mW cm^{-2} sr^{-1} μm^{-1} and $K_2 = 1260.56$ degK, respectively (Schneider and Mauser 1996). Though this is the most popular approach to compute brightness temperature from the observed thermal radiance, other alternatives such as in Singh (1988) and Sospedra *et al.* (1998) have also been proposed.

Landsat TM observed the thermal radiance emitted by the ground at an altitude of about 705 km. When the radiance travels through the atmosphere, it will be attenuated by the absorption of the atmosphere in the wavelength. Moreover, the atmosphere also has ability of emitting thermal radiance. The upwelling atmospheric emittance will combine with the ground thermal radiance to reach the sensor in space. Besides, the ground surface also has ability to reflect the downward atmospheric emittance. These atmospheric impacts in the observed thermal radiance have to be considered when applying Landsat TM6 data for surface temperature estimation and its consequent applications.

3. Correction of brightness temperature for LST retrieval

It has been well known that the impacts of the atmosphere and the emitted ground are unavoidably involved in the sensor-observed radiance. Thus, correction is necessary for retrieving true LST from Landsat TM6 data (Hurtado *et al.* 1996). The correction is based on the radiance transfer equation, which states that the sensor-observed radiance is impacted by the atmosphere and the emitted ground. In accordance with blackbody theory, the thermal emittance from an object can be

expressed as Planck's radiance function:

$$B_\lambda(T) = \frac{C_1}{\lambda^5 (e^{C_2/\lambda T} - 1)} \tag{4}$$

where $B_\lambda(T)$ is the spectral radiance of the blackbody, generally measured in $\mathrm{W\,m^{-2}\,sr^{-1}\,\mu m^{-1}}$, λ is wavelength in metre ($1\ \mathrm{m} = 10^6\ \mu\mathrm{m}$), C_1 and C_2 are the spectral constants with $C_1 = 1.19104356 \times 10^{-16}\ \mathrm{W\,m^2}$ and $C_2 = 1.4387685 \times 10^4\ \mu\mathrm{m}$ degK, T is temperature in degK. The change of Planck's radiance with temperature is shown in figure 1 for TM6.

Blackbody is only a theoretical concept. Most natural surfaces are in fact not blackbodies. Thus, emissivity has to be considered for constructing the radiance transfer equation. Moreover, while transferring from the emitted ground to the remote sensor, the ground emittance is attenuated by the atmospheric absorption. On the other hand, the atmosphere also contributes the emittance that reaches the sensor either directly or indirectly (reflected by the surface). Considering all these components and effects, the sensor-observed radiance for Landsat TM6 can be expressed as:

$$B_6(T_6) = \tau_6[\varepsilon_6 B_6(T_s) + (1-\varepsilon_6) I_6^{\downarrow}] + I_6^{\uparrow} \tag{5}$$

where T_s is land surface temperature, and T_6 is brightness temperature of TM6, τ_6 is atmospheric transmittance and ε_6 is ground emissivity. $B_6(T_6)$ is radiance received by the sensor, $B_6(T_s)$ is ground radiance, $I_6^{\downarrow}$ and $I_6^{\uparrow}$ are the down welling and upwelling atmospheric radiances, respectively.

The upwelling atmospheric radiance $I_6^{\uparrow}$ is usually computed (França and Cracknell 1994, Cracknell 1997) as

$$I_6^{\uparrow} = \int_0^Z B_6(T_z) \frac{\partial \tau_6(z, Z)}{\partial z} dz \tag{6}$$

where T_z is atmospheric temperature at altitude z, Z is altitude of the sensor, $\tau_6(z, Z)$ represents the upwelling atmospheric transmittance from altitude z to the sensor height Z. Following McMillin (1975), Prata (1993) and Coll *et al.* (1994), we employ

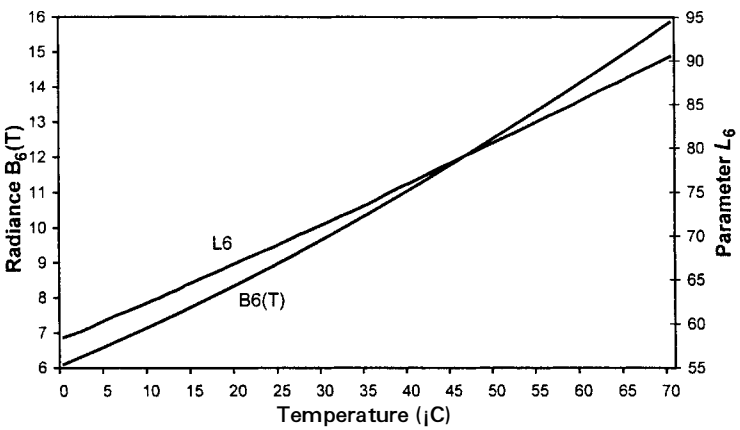

Figure 1. Change of Planck's radiance $B_6(T)$ (*a*) and the parameter L_6 (*b*) with temperature for Landsat TM6.

the mean value theorem to express the upwelling atmospheric radiance as:

$$B_6(T_a)=\frac{1}{1-\tau_6}\int_0^z B_6(T_z)\frac{\partial\tau_6(z,Z)}{\partial z}\,dz \tag{7}$$

where T_a is the effective mean atmospheric temperature and $B_6(T_a)$ represents the effective mean atmospheric radiance with T_a for TM6. Thus, we get:

$$I_6^{\uparrow}=(1-\tau_6)B_6(T_a) \tag{8}$$

The down-welling atmospheric radiance is generally viewed as from a hemispherical direction, hence can be computed (França and Cracknell 1994) as

$$I_6^{\downarrow}=2\int_0^{\pi/2}\int_{\infty}^{0} B_6(T_z)\frac{\partial\tau_6'(\theta',z,0)}{\partial z}\cos\theta'\sin\theta'\,dz\,d\theta' \tag{9}$$

where θ' is the down-welling direction of atmospheric radiance and $\tau_6'(\theta', z, 0)$ represents the down-welling atmospheric transmittance from altitude z to the ground surface. According to França and Cracknell (1994), it is rational to assume that $\delta\tau_6'(\theta', z, 0)=\delta\tau_6(z, Z)$ for the thin layers of the whole atmosphere when the sky is clear. Based on this assumption, application of mean value theorem to equation (9) gives

$$I_6^{\downarrow}=2\int_0^{\pi/2}(1-\tau_6)B_6(T_a^{\downarrow})\cos\theta'\sin\theta'\,d\theta' \tag{10}$$

where $T_a^{\downarrow}$ is the downward effective mean atmospheric temperature. The integration term of this equation can be solved as

$$2\int_0^{\pi/2}\cos\theta'\sin\theta'\,d\theta'=(\sin\theta')^2|_0^{\pi/2}=1 \tag{11}$$

Thus, the downward atmospheric radiance cab be estimated as

$$I_6^{\downarrow}=(1-\tau_6)\ B_6(T_a^{\downarrow}) \tag{12}$$

Substitution into equation (5) gives

$$B_6(T_6)=\varepsilon_6\tau_6 B_6(T_s)+\tau_6(1-\varepsilon_6)(1-\tau_6)B_6(T_a^{\downarrow})+(1-\tau_6)\ B_6(T_a) \tag{13}$$

In order to solve this equation for LST, we need to analyse the effect of $B_6(T_a^{\downarrow})$ on the observed LST by TM6. Due to the vertical difference of atmosphere, the upward atmospheric radiance is generally greater than the downward one. Consequently, $B_6(T_a)$ is greater than $B_6(T_a^{\downarrow})$, or $T_a > T_a^{\downarrow}$. Under the clear sky, the difference between T_a and $T_a^{\downarrow}$ is usually within 5°C, i.e. $|T_a - T_a^{\downarrow}| < 5$°C.

For convenience of analysis, we denote $D'=\tau_6(1-\varepsilon_6)(1-\tau_6)$. Since the emissivity ε_6 is generally 0.96–0.98 for most natural surfaces, the value of D' is very small, mainly depended on τ_6. Provided $\tau_6=0.7$ and $\varepsilon_6=0.96$, we get $D'=0.0084$. The very small value of D' makes the approximate of $B_6(T_a^{\downarrow})$ with $B_6(T_a)$ possible and feasible for the derivation of an algorithm from the above equation.

Before we go on our derivation, we need to simulate the effect of approximating $B_6(T_a^{\downarrow})$ with $B_6(T_a)$ on the change of T_s in equation (13). Since $B_6(T_a) > B_6(T_a^{\downarrow})$, the approximation of $B_6(T_a^{\downarrow})$ with $B_6(T_a)$ would lead to the underestimate of both $B_6(T_s)$ and $B_6(T_a)$ in equation (13) for the fixed $B_6(T_6)$. Consequently, it will lead to the underestimate of T_s. The magnitude of the underestimate of $B_6(T_s)$ and $B_6(T_a)$ in

equation (13) depends on their coefficients in the equation, i.e. ε_6 τ_6 for $B_6(T_s)$ and $(1-\tau_6)[1+\tau_6(1-\varepsilon_6)]$ for $B_6(T_a)$. We consider three cases of $|T_a - T_a^{\circ}|$ and two cases of ε_6 and τ_6 for the simulation, which gives the results shown in table 1. The underestimates of T_s for all cases are quite small. For $|T_a - T_a^{\circ}| = 5^{\circ}$C and $\tau_6 = 0.8$, the approximation of $B_6(T_a^{\circ})$ with $B_6(T_a)$ can only lead to the underestimate of T_s 0.0255°C at $T_s = 20^{\circ}$C and 0.0205°C at $T_s = 50^{\circ}$C. The underestimates of T_s are even smaller for $\tau_6 = 0.7$ (table 1). Therefore, we can conclude that the approximation of $B_6(T_a^{\circ})$ with $B_6(T_a)$ will have an insignificant effect on the estimate of T_s from the above equation. With this approximation, the observed radiance of Landsat TM6 can be expressed as

$$B_6(T_6) = \varepsilon_6 \tau_6 B_6(T_s) + (1-\tau_6)[1+\tau_6(1-\varepsilon_6)]B_6(T_a) \tag{14}$$

which enables us to solve T_s for LST retrieval.

In order to solve T_s from equation (14), we need to linearize Planck's radiance function. Because the change of Planck's radiance with temperature is very close to linearity in a narrow temperature range (say, $<15^{\circ}$C) for a specific wavelength (figure 1), the linearization of Planck's function can be done by Taylor's expansion keeping the first two terms:

$$B_6(T_j) = B_6(T) + (T_j - T)\partial B_6(T)/\partial T = (L_6 + T_j - T)\partial B_6(T)/\partial T \tag{15}$$

where T_j refers to the brightness temperatures ($j=6$), land surface temperature ($j=s$) and mean atmospheric temperature ($j=a$). The parameter L_6 is defined as

$$L_6 = B_6(T)/[\partial B_6(T)/\partial T] \tag{16}$$

in which L_6 has the dimension of temperature in degK. The physical meaning of Taylor's expansion in this case is to expresses the radiance of $B_6(T_j)$ in terms of the radiance $B_6(T)$ with a fixed temperature T. Considering the possible $T_s > T_6 > T_a$ for most cases, we defined T in Taylor's expansion as T_6. Thus, to express the Planck's radiance of T_s and T_a for T_6, we have

$$B_6(T_s) = (L_6 + T_s - T_6)\partial B_6(T_6)/\partial T \tag{17a}$$

$$B_6(T_a) = (L_6 + T_a - T_6)\partial B_6(T_6)/\partial T \tag{17b}$$

$$B_6(T_6) = (L_6 + T_6 - T_6)\partial B_6(T_6)/\partial T) = L_6 \partial B_6(T_6)/\partial T \tag{17c}$$

Substituting into equation (15) and eliminating the term $\partial B_6(T_6)/\partial T$, we obtain

$$L_6 = \varepsilon_6\tau_6(L_6 + T_s - T_6) + (1-\tau_6)[1+(1-\varepsilon_6)\tau_6](L_6 + T_a - T_6) \tag{18}$$

For simplification, we define

$$C_6 = \varepsilon_6 \tau_6 \tag{19}$$

$$D_6 = (1-\tau_6)[1+(1-\varepsilon_6)\tau_6] \tag{20}$$

Thus, we have

$$L_6 = C_6(L_6 + T_s - T_6) + D_6(L_6 + T_a - T_6) \tag{21}$$

For Landsat TM6, we find that L_6 has a relation with temperature close to linearity (figure 1). Thus this property enables us to use the following equation to approximate it for the derivation.

$$L_6 = a_6 + b_6 T_6 \tag{22}$$

where a_6 and b_6 are the coefficients. For the possible temperature range 0–70°C

(273–343 degK) in most cases, the coefficients of equation (22) are approximated as $a_6 = -67.355351$ and $b_6 = 0.458606$, with relative estimate error $REE = 0.32\%$, correlation $R^2 = 0.9994$, T-test $T_{\text{test}} = 162.5$ and F-test $F_{\text{test}} = 108328.6$. Both T-test and F-test are statistically significant at $\alpha = 0.001$, indicating that the approximation is very successful. For the smaller temperature ranges, the relative estimate error (REE) can be even reduced to below 0.13% (table 2). All the equations in table 2 are statistically significant at $\alpha = 0.001$. Therefore, with this relation, we have

$$a_6 + b_6 T_6 = C_6(a_6 + b_6 T_6 + T_s - T_6) + D_6(a_6 + b_6 T_6 + T_a - T_6) \tag{23}$$

Solving for T_s, we obtain the algorithm for LST retrieval from Landsat TM6 data as follows:

$$T_s = [a_6(1 - C_6 - D_6) + (b_6(1 - C_6 - D_6) + C_6 + D_6)T_6 - D_6 T_a]/C_6 \tag{24}$$

Provided that ground emissivity is known, the computation of LST from TM6 data is depended on the determination of atmospheric transmittance τ_6 and effective mean atmospheric temperature T_a. Because this algorithm only requires one thermal band for LST estimation, we term it as a mono-window algorithm in order to distinguish from the split window algorithm used for two thermal channels.

4. Determination of effective mean atmospheric temperature

Though it is difficult to directly measure the *in situ* effective mean atmospheric temperature at the satellite pass, there are several ways to have its estimation for the LST retrieval. Here we intend to follow the method of Sobrino *et al.* (1991) for the estimation, which relates the determination of T_a with water vapour distribution in the atmospheric profile. According to Sobrino *et al.* (1991), the effective mean atmospheric temperature T_a can be approximated as:

$$T_a = \frac{1}{w}\int_0^w T_z \, dw(z, Z) \tag{25}$$

Table 1. Underestimate of T_s by approximating $B_6(T_a^{\infty})$ with $B_6(T_a)$.

	Underestimate of T_s in °C					
	For $\tau_6 = 0.7$ and $\varepsilon_6 = 0.96$			For $\tau_6 = 0.8$ and $\varepsilon_6 = 0.96$		
$T_a^{\infty} - T_a$ in °C	At $T_s = 20$	At $T_s = 35$	At $T_s = 50$	At $T_s = 20$	At $T_s = 35$	At $T_s = 50$
2	0.0087	0.0077	0.0070	0.0100	0.0089	0.0081
3	0.0130	0.0116	0.0105	0.0150	0.0134	0.0121
5	0.0220	0.0196	0.0177	0.0255	0.0227	0.0205

Table 2. Coefficients of parameter L_6 for different temperature ranges.

Range °C	a_6	b_6	REE %	R^2	T_{test}	F_{test}
0–30	−60.3263	0.43436	0.0833	0.9998	186.7	150 147.8
10–40	−63.1885	0.44411	0.0973	0.9997	151.6	100 984.8
20–50	−67.9542	0.45987	0.1225	0.9995	117.5	60 141.8
30–60	−71.9992	0.47271	0.0621	0.9999	223.9	218 819.8

where w is total water vapour content in the atmosphere from ground to the sensor altitude Z, T_z is atmospheric temperature at altitude z, $w(z, Z)$ represents water vapour content between z and Z.

Thus, the determination of T_a requires the *in situ* distribution of atmospheric temperature and water vapour content at each layer of the profile. This is generally unavailable for many studies such as our case. Atmospheric simulation model LOWTRAN 7 provides several standard atmospheres containing the standard distributions of many atmospheric quantities (temperature, pressure, H_2O, CO_2, CO, etc.), which was computed from a number of real atmospheric profile data. Therefore, the standard atmospheres represent the general case of atmospheric conditions (clear sky and without great turbulence) in the corresponding regions (Kneizys *et al.* 1988). These standard atmospheric distributions have been extensively used for atmospheric simulation to estimate the required atmospheric parameters in remote sensing when *in situ* atmospheric profile data is not available (Sobrino *et al.* 1991). Here we attempt to demonstrate that these standard profiles can also be used to combine with local meteorological data for T_a estimation.

In order to determine the effective mean atmospheric T_a, we examine the distributions of water vapour content and atmospheric temperature in the standard atmospheres provided by LOWTRAN 7 model. Figure 2 shows the distribution of water vapour content and its ratio to the total against the altitude. Four standard atmospheres are considered: USA 1976, tropical, mid-latitude summer and mid-latitude

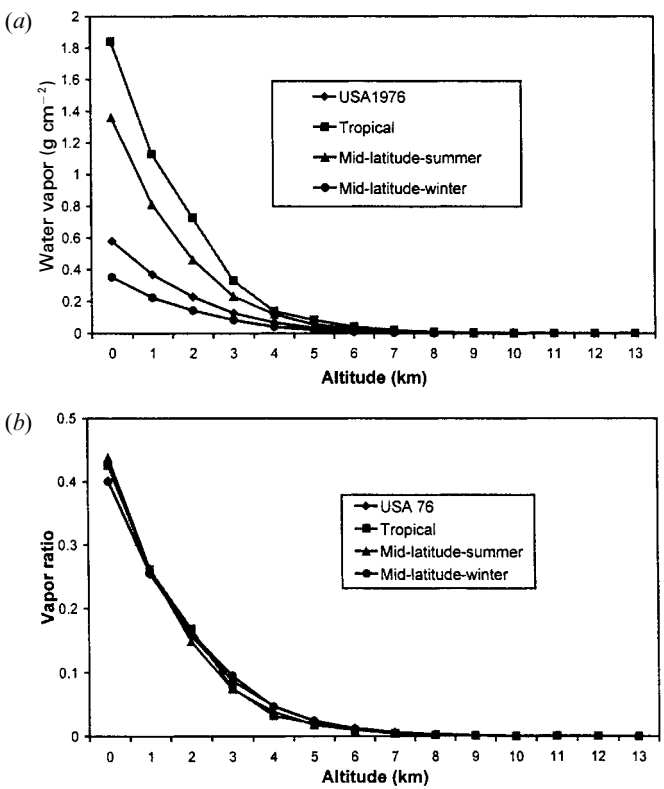

Figure 2. Distribution of water vapour content (*a*) and its ratio to the total, (*b*) against the altitude of the profile.

winter. It is the fact that most atmospheric water vapour is concentrated in the lower atmosphere (Sobrino *et al.* 1991) especially in the first 3 km of the profile (figure 2(*a*)). Though total water vapour content is different (1.44 g cm^{-2} for USA 1976, 4.33 g cm^{-2} for tropical), the distributions of the ratio of water vapour content to the total in the atmospheric profiles are very similar (figure 2(*b*)). The first layer (0–1 km) contains about 40.206% of the total water vapour content in USA 1976, about 43.35% in mid-latitude summer profile. Details of the distributions are given in table 3 for the profiles. Therefore, using the standard distributions of the atmospheres or just their average for simplification, we can develop a simple method to generate the required distribution of the water vapour content at each layer of the atmosphere from the measurement of total water vapour content in the atmosphere as follows:

$$w(z) = wR_w(z) \tag{26}$$

where $w(z)$ is water vapour content at altitude z, $R_w(z)$ is the ratio of water vapour content to the total in the standard atmospheric profiles given in table 3. As indicated by figure 2(*b*) and table 3, the water vapour ratio at the upper layers (>10 km) is negligibly small due to negligibly small water vapour content at the layers (figure 2(*a*)). Thus, at the sensor altitude, we can rationally assume $w(Z) = 0$.

The finite term of equation (25) at altitude z can be approximated as water vapour content of the layer, i.e. $dw(z, Z) = w(z)$. With this approximation, equation (25) can be transformed as

$$T_a = \frac{1}{w} \sum_{z=0}^{m} T_z w(z) \tag{27}$$

where m is number of the atmospheric layers under consideration. Because $w(z)$ in the upper atmospheric layers is very small, the effective mean atmospheric temperature is mainly determined by T_z in the lower atmospheric layers.

It is well known that atmospheric temperature decreases with altitude in the

Table 3. Ratio of water vapour content to the total in different atmospheric profiles.

Altitude (km)	USA 1976	Tropical	Mid-latitude summer	Mid-latitude winter	Average $R_w(z)$
0	0.402058	0.425043	0.438446	0.400124	0.416418
1	0.256234	0.261032	0.262100	0.254210	0.258394
2	0.158323	0.168400	0.148943	0.161873	0.159385
3	0.087495	0.075999	0.074471	0.095528	0.083373
4	0.047497	0.031878	0.038364	0.046510	0.041062
5	0.024512	0.019381	0.017925	0.023711	0.021382
6	0.012846	0.009771	0.009736	0.011514	0.010967
7	0.006250	0.004782	0.005223	0.004092	0.005087
8	0.003132	0.002257	0.002611	0.001471	0.002368
9	0.001049	0.000954	0.001315	0.000587	0.000976
10	0.000358	0.000349	0.000616	0.000238	0.000390
11	0.000142	0.000104	0.000185	0.000060	0.000123
12	0.000055	0.000032	0.000044	0.000026	0.000039
13	0.000023	0.000008	0.000009	0.000016	0.000014
14	0.000009	0.000004	0.000004	0.000011	0.000007
15	0.000006	0.000002	0.000002	0.000008	0.000004

lower atmosphere, i.e. troposphere. Figure 3 perfectly depicts the change of atmospheric temperature and its decrease with altitude for the four atmospheres. Even though the atmospheric temperature of the four profiles differs greatly at the ground surface, it seems that it is very close to each other at about 13 km height (figure 3(*a*)). Atmospheric temperature at this altitude varies from 216.7 degK in USA 1976 through 217 degK in tropical to 218.2 degK in mid-latitude winter profile with an average of 217 degK. With this property, we can compute the decrease rate of atmospheric temperature for the four profiles:

$$R_t(z) = (T_0 - T_z)/(T_0 - 217) \tag{28}$$

where $R_t(z)$ is decrease rate of atmospheric temperature at altitude z and T_0 is atmospheric temperature at the ground. Figure 3(*b*) plots the decrease rate for the four standard atmospheric profiles. Again, figure 3(*b*) indicates that the distributions of the decrease rate are similar with each other. This small variation of the decrease rate in the four different profiles provides the possibility of developing a simple method to generate the distribution of atmospheric temperature T_z for each layer of the atmosphere. Using the distributions of the decrease rate in the standard atmospheres or just their average for simplification, we propose the following formula to

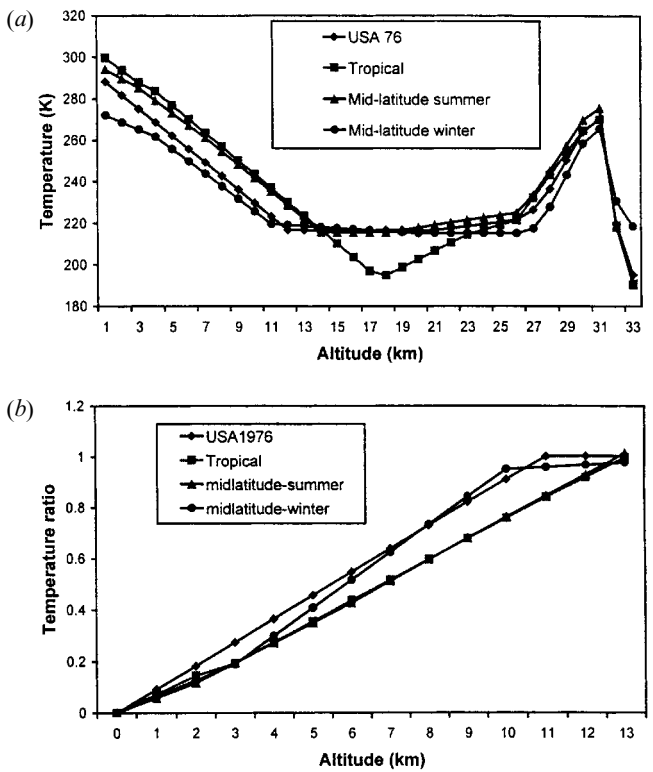

Figure 3. Distribution of atmospheric temperature (*a*) and its attenuation rate, (*b*) against the altitude of the profile.

calculate the distribution of atmospheric temperature from near-surface air temperature for each layer of the atmosphere under consideration in correspondent climate zones:

$$T_z = T_0 - R_t(z)(T_0 - 217) \tag{29}$$

where T_0 is air temperature of the ground (at about 2 m height), $R_t(z)$ is the standard atmospheric temperature decrease rate at z, given in table 4 for correspondent atmospheres.

Therefore, when T_0 is given, the atmospheric temperature distribution at each layer can be directly computed from equation (29). Generally speaking, T_0 is available in local meteorological observation data. Therefore, when the local *in situ* atmospheric profiles of water vapour and atmospheric temperature are not available at the satellite pass, the following procedure can be used to determine T_a for LST retrieval from Landsat TM6 data.

(1) Use available atmospheric profiles of the study region to compute $R_w(z)$ and $R_t(z)$ for water vapour content and atmospheric temperature at each layer and use the average of the ratio and the rates to represent the general atmospheric distribution of the region. If the profiles are also unavailable (such as our case), select one of the standard atmospheric distributions in tables 3 and 4 as the distribution according to the latitude and climate type of the region.

(2) Use equation (26) and the total atmospheric water vapour content to fit into the distribution of water vapour ratio for computation of water vapour content at each layer of the profile. If total atmospheric water vapour content is not available, it can be approximately estimated as $w = w(0)/R_w(0)$ in which $w(0)$ is water vapour content near the surface (at about 2 m height). Usually, we can obtain $w(0)$ from local meteorological data.

(3) Use equation (29) and the known local air temperature near the surface as T_0 to fit into the distribution for computation of atmospheric temperature at each layer.

Table 4. Decrease rate of atmospheric temperature in different profiles.

Altitude (km)	USA 1976	Tropical	Mid-latitude summer	Mid-latitude winter	Average $R_t(z)$
0	0	0	0	0	0
1	0.0912921	0.0725514	0.0582902	0.0634058	0.0713849
2	0.1825843	0.1451028	0.1165803	0.1268116	0.1427697
3	0.2738764	0.1934704	0.1943005	0.1902174	0.2129662
4	0.3651685	0.2744861	0.2720207	0.2989130	0.3026471
5	0.4564607	0.3555018	0.3497409	0.4076087	0.3923280
6	0.5477528	0.4365175	0.4274611	0.5163043	0.4820090
7	0.6390449	0.5163241	0.5116580	0.6250000	0.5730068
8	0.7303371	0.5973398	0.5958549	0.7336957	0.6643069
9	0.8216292	0.6783555	0.6800518	0.8423913	0.7556070
10	0.9115169	0.7581620	0.7629534	0.9510870	0.8459298
11	1.0028090	0.8415961	0.8471503	0.9601449	0.9129251
12	1.0042135	0.9201935	0.9313472	0.9692029	0.9562393
13	1.0042135	1	1.0155440	0.9782609	0.9995046
14	1.0042135	1.0810157	1.0168394	0.9873188	1.0223469
15	1.0042135	1.1608222	1.0168394	0.9963768	1.0445630

(4) Use equation (28) to compute the effective mean atmospheric temperature T_a through summation of atmospheric temperature multiplied with water vapour content at each layer for the whole profile.

When using the standard atmospheric distribution of water vapour content and temperature given in tables 3 and 4, one should remember that it involves the basic assumption that the sky is clear and there is not great vertical turbulence in the atmosphere (Kneizys *et al.* 1988). This assumption is very important because turbulence in the atmosphere may produce a great change in the distribution of water vapour content and atmospheric temperature at each layer, which consequently makes the estimation of T_a obviously biased.

Actually, with the above standard distributions of water vapour content and atmospheric temperature, we can further derive a simpler formula for approximation of T_a. From equation (27), we obtain

$$T_a = \Sigma T_z w(z)/w = \Sigma T_z R_w(z) \tag{30}$$

This formula implies that T_a is dependent on the distributions of both water vapour rate and air temperature in the atmosphere. Replacing T_z with formula (29), we obtain

$$\begin{aligned} T_a &= \Sigma(T_0 - R_t(z)(T_0 - 217))R_w(z) \\ &= \Sigma T_0 R_w(z) - \Sigma T_0 R_t(z) R_w(z) + \Sigma 217 R_t(z) R_w(z) \\ &= T_0(\Sigma R_w(z) - \Sigma R_t(z) R_w(z)) + 217 \Sigma R_t(z) R_w(z) \end{aligned} \tag{31}$$

With the standard distributions given in tables 3 and 4, we derive the simple linear relations for approximation of T_a from T_0 for the four standard atmospheres as follows:

$$\text{For USA 1976} \qquad T_a = 25.9396 + 0.88045 T_0 \tag{32a}$$

$$\text{For tropical} \qquad T_a = 17.9769 + 0.91715 T_0 \tag{32b}$$

$$\text{For mid-latitude summer} \qquad T_a = 16.0110 + 0.92621 T_0 \tag{32c}$$

$$\text{For mid-latitude winter} \qquad T_a = 19.2704 + 0.91118 T_0 \tag{32d}$$

where both T_a and T_0 are with dimension in K. These formulae imply that, under the standard atmospheric distributions (clear sky and without great turbulence), the effective mean atmospheric temperature T_a is a linear function of near-surface air temperature T_0. This is because the impacts of water vapour distribution and atmospheric temperature distribution on T_a are assumed to be constant for the standard distributions.

Once T_a has been calculated, the LST can be retrieved using the mono-window algorithm described in equation (24) when the atmospheric transmittance is given.

5. Determination of atmospheric transmittance

Provided ε_6 available and T_a determined, atmospheric transmittance now becomes the only parameter unknown for the algorithm. Generally speaking, the determination of atmospheric transmittance for Landsat TM6 is undertaken through the simulation of atmospheric conditions using such atmospheric simulation programs as LOWTRAN, MODTRAN or 6S. Due to its extreme importance in influencing the variation of atmospheric transmittance, water vapour content has

been extensively used as the determinant in estimation of atmospheric transmittance (Sobrino *et al.* 1991, Coll *et al.* 1994, Cracknell 1997).

In the study, LOWTRAN 7 program is used to simulate the relation of water vapour content to atmospheric transmittance. The general water vapour range of 0.4–4.0 g cm^{-2} is considered for the simulation under two profiles: low and high temperature profiles. The atmospheric temperature near the surface for the high temperature profile is defined as 35°C and for the low one, 18°C. The swath of Landsat TM is about 185 km, which results in a viewing zenith angle of about 6° for its edge pixels. Thus, we consider an average zenith angle of 3° for the simulation of atmospheric impact on transmittance. Simulation results are shown in figure 4, from which we can see that TM6 transmittance decreases steadily with water vapour content increase. Atmospheric transmittance of TM6 is high up to above 0.9 for water vapour content less than 0.8 g cm^{-2}. The transmittance decreases to about 0.8 at 2.0 g cm^{-2} and 0.7 at 2.5 g cm^{-2}. It may be lower than 0.5 for water vapour content greater than 4.0 g cm^{-2}. Another feature shown in figure 4 is the transmittance difference between the two profiles. The difference is very small when water vapour content is low. However, it increases rapidly with the water vapour content. High temperature profile has higher transmittance than low temperature profile for the same water vapour content. The transmittance difference between high and low temperature profiles is about 0.007 at water vapour content 1 g cm^{-2}. The difference increases to 0.031 at 2 g cm^{-2}, 0.0558 at 3 g cm^{-2} and 0.0799 at 4 g cm^{-2}. The change of transmittance with water vapour is not linear for the whole range 0.4–4 g cm^{-2} but for a small segment the relationship is close to linearity. This characteristic provides the possibility of establishing some simple linear equations to estimate transmittance from water content for Landsat TM6 operating in 10.5–12.5 μm. An effort of establishing the estimation equations is given in table 4 for the range 0.4–3 g cm^{-2}, which is the general case.

The estimation equations listed in table 5 have high squared correlation and low standard error, which means that the estimation of transmittance with water vapour content by these equations will have a high accuracy. For a possible measurement error of 0.2 g cm^{-2} (this is the general accuracy of water vapour content estimation

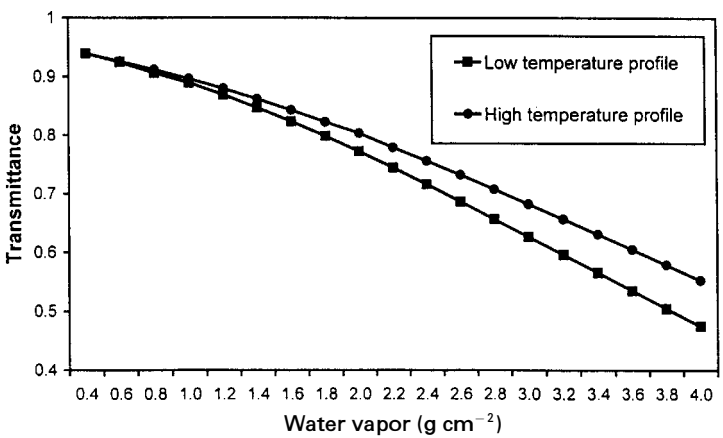

Figure 4. Change of atmospheric transmittance with water vapour content for Landsat TM6.

Table 5. Estimation of atmospheric transmittance for Landsat TM channel 6.

Profiles	Water vapour (w) ($g\,cm^{-2}$)	Transmittance estimation equation	Squared correlation R^2	Standard error
High air temperature	0.4–1.6	$\tau_6 = 0.974290 - 0.08007w$	0.99611	0.002368
	1.6–3.0	$\tau_6 = 1.031412 - 0.11536w$	0.99827	0.002539
Low air temperature	0.4–1.6	$\tau_6 = 0.982007 - 0.09611w$	0.99463	0.003340
	1.6–3.0	$\tau_6 = 1.053710 - 0.14142w$	0.99899	0.002375

from sunphotometer measurements), the possible maximal estimation error of atmospheric transmittance for Landsat TM6 is <0.029. An accurate estimation of transmittance, as indicated in following section, is very important in retrieval of LST from Landsat TM6 data.

6. Sensitivity analysis of the mono-window algorithm

The mono-window algorithm for Landsat TM requires three critical parameters to estimate LST: ground emissivity, atmospheric transmittance and effective mean atmospheric temperature. Due to many difficulties such as unavailability of precise profile data about the atmosphere and the complexity of the emitted ground surface in terms of material composition, the determination of these parameters will unavoidably involve some errors. In order to analyse the impact of the possible estimation error of these critical parameters on the possible LST estimation error, sensitivity analysis is necessary. For convenience, the following formula is used to express the possible LST estimation error:

$$\delta T_s = |T_s(x + \delta x) - T_s(x)| \tag{33}$$

where δT_s is LST estimation error, x is the variable to which the sensitivity analysis orients (ε_6, τ_6 and T_a), δx is possible error of the variable x, $T_s(x+\delta x)$ and $T_s(x)$ are the LST simulated by our algorithm in equation (24) for $x+\delta x$ and x respectively.

Sensitivity analysis is performed under several conditions. First of all, natural surfaces generally have an emissivity of about 0.95–0.98 in the thermal wavelength 10–13 μm (Price 1984, Sutherland 1986, Takashima and Masuda 1987). We assume an emissivity of 0.97 for the sensitivity analysis. Secondly, a clear sky is very important and we assumed a transmittance of 0.80 for the analysis. The overpass of Landsat 5 in many regions was at about 9:30–10:00 am local time when the atmospheric temperature is generally not very high. Thus, the effective mean temperature is arbitrarily given as 15°C. The air temperature near the surface corresponding to this mean temperature is about 25°C for water vapour content of about $2\,g\,cm^{-2}$. Under these conditions, we perform the sensitivity analysis of the mono-window algorithm for estimation errors of ground emissivity, transmittance and effective mean atmospheric temperature.

Figure 5 illustrates the probable LST estimation error due to the possible ground emissivity error. Several important features can be seen in figure 5(*a*), which plots the LST estimation error against brightness temperature of TM6 for the four possible emissivity errors. LST estimation error δT decreases with brightness temperature increase when it is below 13°C, which is a transition point. From this point, δT increases rapidly with temperature in all cases. Linear correlation between LST error

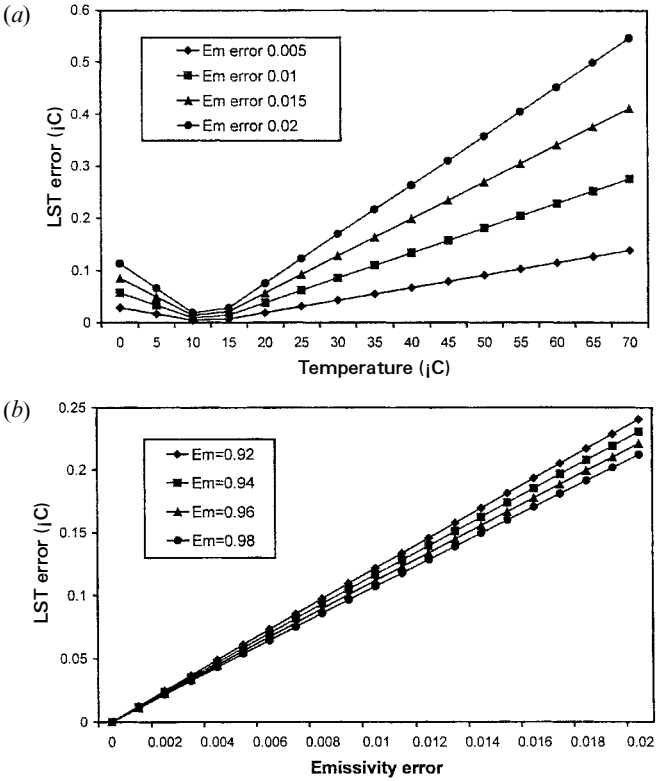

Figure 5. Probable LST estimation error due to the possible emissivity error. (*a*) LST error against brightness temperature, and (*b*) average LST error against emissivity error.

and temperature is also very clear in all the cases. According to these relationships, we can expect that δT is less than 0.2°C for $\delta\varepsilon_6 = 0.01$ and 0.4°C for $\delta\varepsilon_6 = 0.02$ in temperature range 0–55°C (figure 5(*a*)). This LST estimation error corresponding to emissivity error is relatively small. Generally, the estimation of ground emissivity in the range of 10–13 μm can reach an accuracy of less than 0.02. Provided this assumption, the mono-window algorithm is able to produce a quite accurate LST estimation from Landsat TM6 data in spite of some possible emissivity errors.

Considered the most possible temperature in many regions, an average δT in temperature range of 10–55°C has been plotted against the possible $\delta\varepsilon_6$ (figure 5(*b*)). Four ground emissivity cases are plotted in figure 5(*b*), which indicates that the LST error has very small change with the ground emissivity. This means that δT is only sensible to emissivity error but not to the level of ground emissivity itself. For $\delta\varepsilon_6 = 0.02$, δT is 0.24°C at $\varepsilon_6 = 0.92$ and 0.22°C at $\varepsilon_6 = 0.98$, with a negligible difference of about 0.02°C (figure 5(*b*)). This little change of δT with ε_6 supports our above conclusion about the applicability of the algorithm in many cases.

In contrast with the insensible response to emissivity error, the algorithm is quite sensible with transmittance error. Figure 6 shows the probable LST estimation error δT due to possible transmittance error $\delta\tau_6$. Again, δT is 0 at brightness temperature level of about 13°C for all cases of transmittance error (figure 6(*a*)). When brightness temperature is below this level, δT is less than 0.25°C for $\delta\tau_6 \leqslant 0.02$. However, δT increases rapidly with temperature and transmittance. For $\delta\tau_6 = 0.02$, δT is about

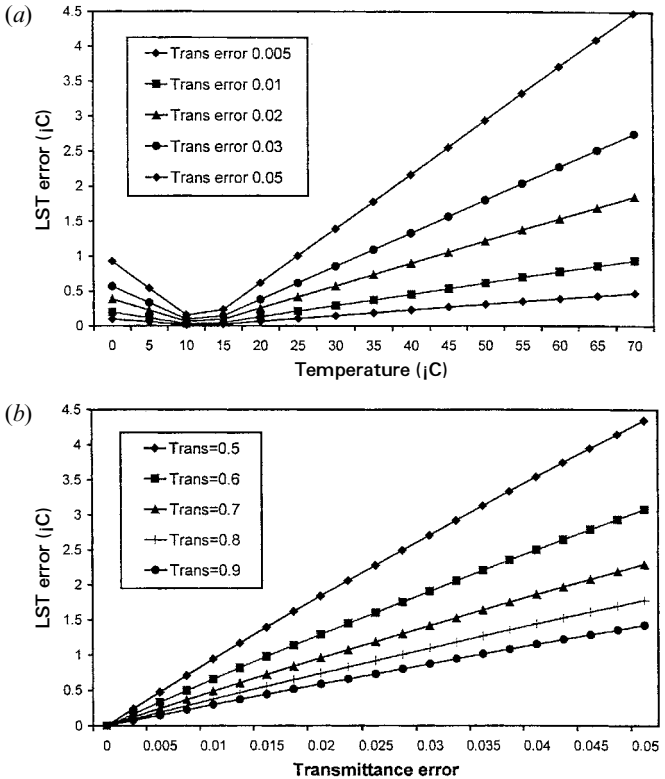

Figure 6. Probable LST estimation due to the possible atmospheric transmittance error. (*a*) LST error against brightness temperature, and (*b*) average LST error against transmittance error.

0.577°C at temperature $T=30$°C and it increases to abut 1.058°C at $T=45$°C and 1.378°C at $T=55$°C (figure 6(*a*)). For $\delta\tau_6=0.025$, δT may reach above 3°C at $T>45$°C. Therefore, an accurate estimation of atmospheric transmittance is much more important in using the algorithm for LST retrieval than the emissivity estimation.

Moreover, δT is also very sensible to the change of atmospheric transmittance (figure 6(*b*)). Average LST error in the temperature range of 10–55°C is plotted against transmittance error for several transmittance levels. When transmittance is high, the increase of average δT against $\delta\tau_6$ is much slower. Specifically, average δT is about 0.74–0.96°C for $\delta\tau_6=0.02$ when τ_6 is within 0.7–0.8. For the same $\delta\tau_6$, the average δT increases to 1.29–1.84°C when τ_6 decreases to 0.5–0.6. Generally speaking, the accuracy of atmospheric water vapour measurement is about $\leqslant 0.2\,\mathrm{g\,cm^{-2}}$. Consequently it produces an error of 0.016–0.28 in τ_6 estimation (table 4). Therefore, we can expect that the algorithm is able to provide a LST estimation with an error <1°C for $\tau_6>0.7$. This accuracy is generally acceptable for most study purposes using Landsat TM6 data (Kerr *et al.* 1992).

Sensitivity analysis of the algorithm to effective mean atmospheric temperature T_a indicates that δT does not change with brightness temperature and the mean atmospheric temperature itself but does change linearly with the possible error of the mean temperature. This can be understood through the derivation of the LST

estimation error δT according to equation (33). For a small error of T_a, we can derive that

$$\begin{aligned}\delta T &= |T_s(T_a+\delta T)-T_s(T_a)| \\ &= |\{[a_6(1-C_6-D_6)+(b_6(1-C_6-D_6)+C_6+D_6)T_6-D_6(T_a+\delta T_a)]/C_6\} \\ &\quad -\{[a_6(1-C_6-D_6)+(b_6(1-C_6-D_6)+C_6+D_6)T_6-D_6T_a]/C_6\}| \\ &= |[D_6T_a-D_6(T_a+\delta T_a)]/C_6| \\ &= |(D_6/C_6)\delta T_a| \end{aligned} \tag{34}$$

For a given emissivity and transmittance, parameters C_6 and D_6 are fixed according to equations (19) and (20). Therefore, δT only varies with δT_a but not T_6 or T_a itself. In order to analyse the change of δT with δT_a, we compute the ratio of D_6 to C_6 for several combinations. The results are given in table 6, which indicates that the ratio D_6/C_6 is mainly dependent on transmittance though emissivity has slightly effect on it. The ratio changes from 0.259 for $\varepsilon_6=0.98$ to 0.279 for $\varepsilon_6=0.94$ with an average of 0.269 when the transmittance is 0.8. It changes in the range of 0.443–0.475 for the emissivity range 0.94–0.98 when $\tau_6=0.7$. Based on the average ratio of the combinations for different transmittances, we plot the change of δT against δT_a in figure 7.

Figure 7 indicates that LST estimation error increases rapidly with the possible mean atmospheric temperature error and the average ratio D_6/C_6, which is mainly dependent on transmittance (table 5). When mean atmospheric estimation error is about 1°C, the probable LST estimation error is about 0.27°C for the average ratio $D_6/C_6=0.27$ which corresponds to $\tau_6=0.8$. However, the δT may reach up to 0.71°C for the same δT_a but the ratio $D_6/C_6=0.71$ or $\tau_6=0.6$. If δT_a is greater than 2°C,

Table 6. Comparison of the ratio D_6/C_6 for different combinations.

Emissivity	Transmittance	Parameter C_6	Parameter D_6	Ratio D_6/C_6	Average ratio
0.94	0.6	0.564	0.4144	0.734752	
0.95	0.6	0.570	0.4120	0.722807	
0.96	0.6	0.576	0.4096	0.711111	0.711352
0.97	0.6	0.582	0.4072	0.699656	
0.98	0.6	0.588	0.4048	0.688435	
0.94	0.7	0.658	0.3126	0.475076	
0.95	0.7	0.665	0.3105	0.466917	
0.96	0.7	0.672	0.3084	0.458929	0.459093
0.97	0.7	0.679	0.3063	0.451105	
0.98	0.7	0.686	0.3042	0.443440	
0.94	0.8	0.752	0.2096	0.278723	
0.95	0.8	0.760	0.2080	0.273684	
0.96	0.8	0.768	0.2064	0.268750	0.268852
0.97	0.8	0.776	0.2048	0.263918	
0.98	0.8	0.784	0.2032	0.259184	
0.94	0.9	0.846	0.1054	0.124586	
0.95	0.9	0.855	0.1045	0.122222	
0.96	0.9	0.864	0.1036	0.119907	0.119955
0.97	0.9	0.873	0.1027	0.11764	
0.98	0.9	0.882	0.1018	0.11542	

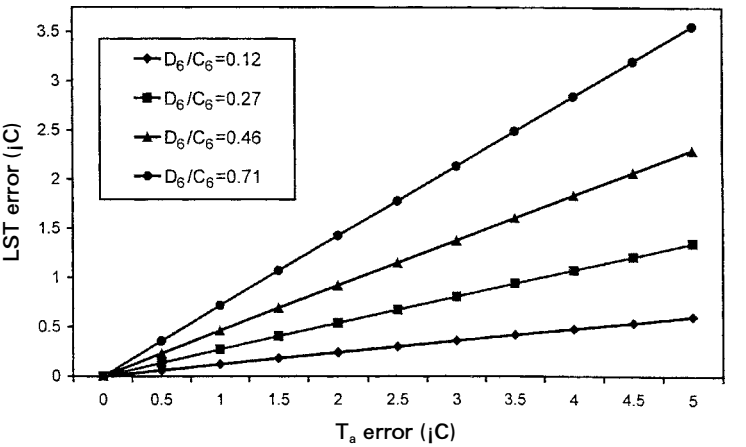

Figure 7. Probable LST estimation error due to the possible mean atmospheric temperature error.

the δT is about 0.54°C for $\tau_6 = 0.8$ and about 0.91°C for $\tau_6 = 0.7$. Therefore, the accurate estimation of mean atmospheric temperature is very important for an accurate LST retrieval from the only one thermal band of Landsat TM data. When $\tau_6 < 0.65$ and $\delta T_a > 2$°C, an obvious LST estimation error (>1°C) is generally unavoidable. However, if the sky is very clear so that $\tau_6 > 0.8$, the possible δT will be less than 1°C for δT_a of high up to 4°C. And such a big δT_a rarely happens in the real world. Therefore, a clear sky with lower water vapour content is an ideal atmospheric condition for remote sensing of LST with Landsat TM6 data.

7. Validation of the algorithm

The sensitivity analysis is to provide an assessment of the relative accuracy of the algorithm, i.e. the effect of possible error in parameter estimation on the LST retrieval. Validation of the algorithm is also necessary in order to understand how well the retrieved LST with the algorithm matches to the actual one in the real world.

The best way to validate the algorithm is to compare the *in situ* ground truth measurements of LST with the retrieved ones with the algorithm from the Landsat TM6 data of a specific region. However, this is not feasible because it is extremely difficult to obtain the *in situ* ground truth measurements comparable to the pixel size of Landsat TM6 data at the satellite pass. An alternative or the practical way is to use the simulated data generated by atmospheric simulation programs such as LOWTRAN, MODTRAN or 6S. These programs can simulate the thermal radiance reaching the remote sensor at the satellite level for the input profile data with the known ground thermal properties (LST and emissivity). The required atmospheric quantities such as transmittance for remote sensing of LST is also able to compute from the output of the simulation with the programs. The simulated total radiance can be used to convert into the brightness temperature for TM6. Then, the LST can be estimated with our mono-window algorithm. Comparison of the assumed LST used for the simulation with the retrieved one from the simulated total radiance enables us to examine the accuracy of the algorithm for the true TM6 data.

The validation of our algorithm was done through simulation with LOWTRAN 7.0 (Kneizys *et al.* 1988). A number of situations were designed for the validation.

Four land surface temperatures (20°C, 30°C, 40°C and 50°C) with four correspondent surface air temperatures (18°C, 23°C, 30°C and 38°C) were arbitrarily assumed for the simulation. Seven atmospheric profiles were used: USA1976 from LOWTRAN 7.0 as well as the tropical 15° N, the subtropical 30° N July and January, and the mid-latitude 45° N July and January given in Cole *et al.* (1965). For any combination of these temperatures and profiles, five cases of total water vapour content (1 g cm^{-2}, 2 g cm^2, 2.5 g cm^{-2}, 3 g cm^{-2}, and 3.5 g cm^{-2}) were considered. Since most natural surfaces of the Earth have emissivity of 0.95–0.98, we used $\varepsilon_6 = 0.965$ for the simulation.

In actual operation, the atmospheric temperature and water vapour profile data were first estimated for each situation according to the distributions of these atmospheric profiles. Second, the LOWTRAN 7.0 program was run for radiance and transmittance. The outputs were then used to compute the total thermal radiance and atmospheric transmittance for TM6. Brightness temperature was converted from the total thermal radiance using Planck's function for each situation. This brightness temperature was finally used to put into our mono-window algorithm for LST retrieval. The difference between the assumed LST for the simulation and the retrieved one represents how good the algorithm works in LST retrieval from TM6 data.

Table 7 lists the detailed results of the validation for USA1976 atmosphere with the total water vapour 2.5 g cm^{-2}. Table 8 gives the main results for all situations used in the simulation. The results shown in both tables 7 and 8 indicate the algorithm is able to provide a quite accurate estimate of LST in most cases. The LST difference between the assumed and the retrieved ones are less than 0.4°C in most cases. In many regions, the satellite overpass was at 9:00–10:00 am when the ground surface is not very hot. Usually the LST at this time is less than 40°C in many cases. Provided this condition, the LST difference is even smaller. For instance, the LST difference is only about 0.23°C for mid-latitude summer atmosphere with total water vapour content up to 2.5 g cm^{-2} and a LST up to 40°C. This good matching of the retrieved LST to the actual one confirms the applicability of the mono-window algorithm.

8. Spatial variation of LST in the Israel-Egypt border region

In order to provide an example of the algorithm's application, we used it to retrieve LST from Landsat TM6 data of the Israel–Egypt border region where an interesting thermal phenomenon was found across the border. The geomorphological structure is the same on both sides of the border, that is the linear sand dunes stretching from south to north. Fine sand with a diameter of about 0.05–0.5 mm is the principal material of soil constituents in the region though silt and clay also

Table 7. Validation of the algorithm for the USA 1976 atmosphere.

LST T_s (°C)	Estimated T_a (°C)	Simulated $B_6(T_6)$ (W m^{-2} sr^{-1} μm^{-1})	Simulated T_6 (°C)	Transmittance τ_6	Retrieved LST T_s' (°C)	Difference $T_s' - T_s$ (°C)
20	9.132	7.8865	15.568	0.701747	20.128	0.128
30	13.534	8.9523	24.126	0.721060	30.283	0.283
40	19.697	10.1903	33.392	0.744298	40.371	0.371
50	26.741	11.5488	42.890	0.761250	50.421	0.421

Table 8. Main results of validating the algorithm for various situations.

Water vapour content ($g\,cm^{-2}$)	LST T_s (°C)	LST difference $T_s' - T_s$ (°C)					
		USA 1976	Tropical	Sub-tropical July	Sub-tropical January	Mid-latitude July	Mid-latitude January
	20	0.049	0.024	0.028	0.018	0.019	0.027
1	30	0.114	0.075	0.082	0.066	0.067	0.081
	40	0.151	0.105	0.114	0.094	0.095	0.112
	50	0.173	0.121	0.131	0.109	0.110	0.129
	20	0.098	0.046	0.055	0.035	0.035	0.053
2	30	0.213	0.137	0.151	0.120	0.121	0.149
	40	0.285	0.196	0.212	0.175	0.176	0.209
	50	0.333	0.232	0.251	0.209	0.210	0.248
	20	0.128	0.060	0.072	0.045	0.046	0.07
2.5	30	0283	0.181	0.200	0.158	0.160	0.197
	40	0.371	0.254	0.276	0.227	0.229	0.272
	50	0.421	0.293	0.316	0.263	0.265	0.313
	20	0.161	0.075	0.090	0.057	0.058	0.088
3	30	0.353	0.226	0.249	0.197	0.199	0.245
	40	0.462	0.315	0.342	0.282	0.284	0.338
	50	0.502	0.349	0.377	0.314	0.316	0.373
	20	0.181	0.084	0.101	0.064	0.065	0.099
3.5	30	0.388	0.248	0.274	0.216	0.218	0.269
	40	0.516	0.352	0.382	0.314	0.316	0.377
	50	0.421	0.293	0.316	0.263	0.265	0.313

accounts some percentages of the surface layer especially on the Israeli side where a thin biogenic crust (1–5 mm) covers most of its surfaces. Average annual rainfall of the region is 95 mm (Kidron and Yair 1997).

On the Egyptian side (Sinai), the region is under intensive use by Bedouin nomads, who use the sand surface for grazing goats, camels and other cattle as well as some activities of cropping. High plants (shrubs) have been subjected to severe gathering for firewood (Tsoar and Møller 1986). In contrast to the free-use in the Egyptian side, the Israeli side (Negev) has been managed under strict conservation policies. The limited anthropogenic activities on the Israel side have led to the establishment of vegetation (shrubs and annuals) and biogenic crust (composed of lichen, fungi and other microphytes especially chlorophyll-containing cyanobacteria) on the surface of the sand dune region (Karnieli 1997).

The difference in land use between Israel and Egypt has a pronounced effect on remote sensing imagery. On the image of visible bands, a sharp spectral contrast can be seen between the Egyptian Sinai and the Israeli Negev (Karnieli and Tsoar 1995, Tsoar and Karnieli 1996, Karnieli 1997). The relatively higher reflectance value of the remote sensing image on the Egyptian side was believed to be directly resulted from severe anthropogenic impact of the Sinai Bedouin, including overgrazing and firewood gathering (Tsoar and Møller 1986).

The contrast between the two sides of Israel-Egypt border is also observed in the thermal channel of remote sensing data such as NOAA-AVHRR and Landsat TM. The Israeli side has obviously higher brightness temperature on both AVHRR and TM images. Because bare sand usually has lower ground emissivity than biogenic crust, we still do not know if the Israeli side really has higher LST than the Egyptian

side. In order to answer this question and analyse the spatial patterns of the thermal variation in the border region, we apply the above mono-window algorithm to the available Landsat-5 TM images.

Figure 8 represents one result of the efforts, which shows the spatial variation of LST distribution in the region. This image was taken on 29 March 1995, which is in the blooming season. The satellite Landsat-5 passed the area at about 9:30 am. According to the measurement of CIMEL sunphotometer on the roof of our laboratory at Sede Boker, about 30 km from the region, the water vapour content in the atmospheric profile was 1.185 g cm^{-2} at the pass. By this water vapour content, we estimate the atmospheric transmittance was about 0.8681 at the time when the image was acquired. Data from Meteorological Observation Station at Sede Boker indicates that air temperature near the surface at about 9:30 am of the date was 14.5°C. Thus, the effective mean atmospheric temperature was estimated to be 7.17°C at the satellite pass. According to our experiments with samples taken from the field, the biogenic crust has an average emissivity of about 0.97 and the bare sand 0.95. Using the sharp contrast on both sides in the visible channels, we assign the emissivity difference to the pixels according to its DN value.

The LST images produced from the retrieval efforts demonstrate that a sharp difference of LST does exist across the border (figure 8). Generally speaking, the Israeli side has an obvious higher LST than the Egyptian side. On average, LST is 34.33°C on the Israeli side and 30.95°C on the Egyptian side. Thus the difference is about 3.38°C. This LST difference can also be clearly seen on the image (figure 8). The highest LST mainly distributes on the Israeli side in the right upper corner of the image. The LST in this area is high up to 35–37°C. Low LST mainly concentrates

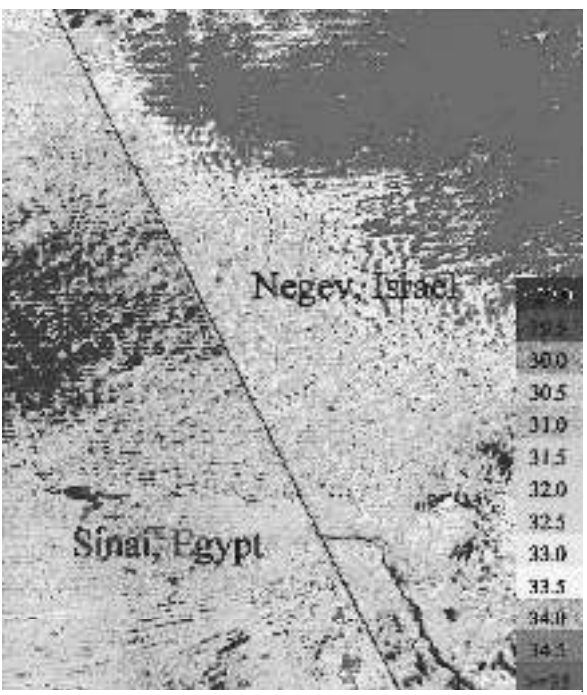

Figure 8. Land surface temperature variation in the sand dunes across the Israel–Egypt border, retrieved from Landsat TM6 data of 29 March, 1995.

in the middle part of the Egyptian side. The LST in this part is only about 28–29°C. LST in the area close to the border is about 31–33°C on Israeli side and 29–30°C on Egyptian side. Sharp contrast of LST can still be distinguished in this area next to the border on both sides even though the difference is lower than the average one. This contrast of LST distribution on both sides makes the border very clearly seen in the sand dune region.

Considered more vegetation cover on the Israeli side and the blooming season, the higher LST on the Israeli side is really interesting. The main reason is that the Israeli side has much higher biogenic crust cover while the Egyptian side is dominant with much more bare sand. Biogenic crust cover on the Israeli side is estimated to reach above 72% and bare sand on the Egyptian side is above 80%. Due to low albedo, the biogenic crust usually has much higher surface temperature than the bare sand. Our ground truth measurements indicate that surface temperature on biogenic crust is about 2–3°C higher than that on bare sand (figure 9). The measurements were carried out in the Nizzana research site close to the border on the Israeli side. The time required for the measurements was controlled within an hour so that the effect of measurement time is minimized. Figure 9 indicates that the average LST difference between biogenic crust and bare sand was 2.23°C on 19 March (figure 9(*a*)) and 2.85°C on 26 March,1997 (figure 9(*b*)). Therefore, the higher LST on the Israeli

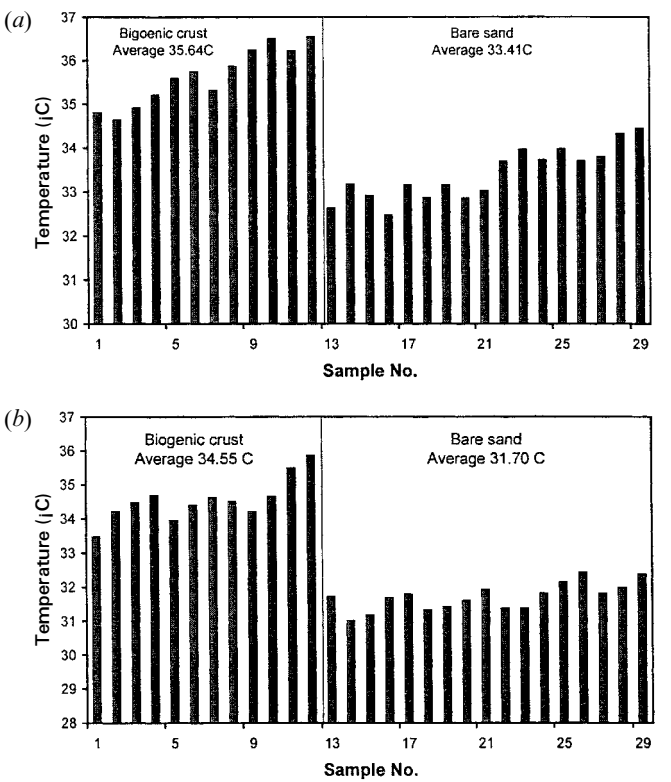

Figure 9. Comparison of land surface temperature on biogenic crust and bare sand in the sand dunes across the Israel–Egypt border. These ground truth measurements were taken on the Israeli side with a hand-hold radiant thermometer (*a*) at 11:16–12:04 on 19 March, 1997 (*b*) and at 11:20–12:00 on 26 March, 1997.

side is due to the contribution of biogenic crust overcoming the cooling process of its higher vegetation cover. Detailed examination of this mechanism is given in another paper.

Due to the probable errors in estimating the key parameters for the LST retrieval, some possible errors may unavoidably involve in this image. We need to evaluate the accuracy of LST estimation in the image according to the possible error in the parameter estimation. As mentioned in above sensitivity analysis, ground emissivity error has slight effect on LST error. Considered a possible error of 0.01 in emissivity estimation, i.e. the emissivity for bare sand in the range of 0.94–0.96 and for biogenic crust 0.96–0.98, the possible LST estimation error is about 0.12°C in the image (figure 5(*b*)). According to Price (1984), Takashima and Masuda (1987) and Humes *et al.* (1993), this estimation of emissivity in the range is reasonable. Therefore, we can conclude that the possible LST error contributed by possible emissivity error is very small.

For the LST error contributed from transmittance error, we consider a moderate error of water vapour measurement in $0.1\,g\,m^{-2}$. At this measurement error, we expect a transmittance error of less than 0.015 according to the equation given in table 4 for the water vapour range $0.4–1.6\,g\,cm^{-2}$. The average LST error due to this transmittance error is less than 0.5°C for transmittance of 0.85 (figure 6(*b*)). Because the effective mean atmospheric temperature is difficult to have an accurate estimation, we consider an error of up to 2.5°C at our T_a determination. With this T_a error, the LST estimation error is about 0.48°C for transmittance of 0.85. A simple summation of these error components gives the probable error of our LST retrieval less than 1.1°C in the image (figure 8). This error is within the generally accepted level 1.5°C (Kerr *et al.* 1992, Li and Becker 1993). If the possible mutual compensation of these error components is considered, the LST distribution shown in this image is even closer to the actual one.

9. Conclusion

Landsat TM images have been extensively applied for various studies of the Earth's resources due to its high spatial resolution. However, the thermal band data of the remote sensor still remains an ignored area in comparison with the extensive applications of its other bands in visible and NIR ranges. One of the main reasons probably is the difficulties of atmospheric correction for LST retrieval from the single thermal band data, The spatial resolution of the Landsat TM thermal band is about $120\,m \times 120\,m$. Even though this spatial resolution is much lower than its visible and NIR channels, it is quite large for analysing the spatial patterns of thermal phenomenon in a macro-scale region.

A mono-window algorithm has been developed in the study for the retrieval of LST from Landsat TM6 data, which is assumed to be reliable though radiometric calibration is necessary for many applications. The derivation of the algorithm is based on the thermal radiance transfer equation and the linearization of Planck's radiance function. Totally there are three critical parameters in the algorithm: emissivity, transmittance and mean atmospheric temperature. If these three parameters are given, it is very easy to use this algorithm for LST estimation from Landsat TM6 data. The principle of algorithm can be also extended to other sources of one-thermal-channel data for LST retrieval.

The determination of ground emissivity is a complicated issue and there is a great volume of literature addressing it. Generally, the change of atmospheric

transmittance is mainly depended on the variation of water vapour content in the profile. This characteristic has been widely used to determine the atmospheric transmittance through the simulation with such programs as LOWTRAN or MODTRAN. Based on the simulation results with LOWTRAN 7 program, equations have been established for estimation of atmospheric transmittance from water vapour content in the general range 0.4–3.0 g cm^{-2} for Landsat TM6 data. These equations can provide quite accurate estimation of transmittance if the measurement of water vapour content is accurate.

A practicable and simple method has been proposed for estimation of the required effective mean atmospheric temperature for LST retrieval using the mono-window algorithm. When the *in situ* profile at satellite pass is available, the computation of the mean atmospheric temperature can be easily done with the equation (22) proposed by Sobrino *et al.*(1991). However, this is not the general case. Study of different standard profiles indicates that the distributions of water vapour and temperature in the atmospheres are quite similar when the sky is very clear and there is no great turbulence. With this similarity, a method is proposed for the calculation of the mean atmospheric temperature from local meteorological observation data, which is usually accessible. Therefore, when the profile is not available, water vapour content and atmospheric temperature at each layer can be approximated using the local meteorological observation data to fit into the standard distributions of the climate zone.

Usually it is very difficult to reach an accurate estimation of ground emissivity in spite of several methods have been proposed (Li and Becker 1993, Humes *et al.* 1994). Fortunately, results from sensitivity analysis of the algorithm indicates that the probable LST estimation error δT due to ground emissivity error $\delta\varepsilon_6$ is much lower than the LST error due to transmittance error $\delta\tau_6$ and mean atmospheric temperature error δT_a. On average, probable δT is less than 0.12°C for $\delta\varepsilon_6 < 0.01$ and 0.24°C for $\delta\varepsilon_6 < 0.02$. Moreover, LST error slightly changes with emissivity for the same $\delta\varepsilon_6$. On the other hand, LST error is sensible to the transmittance error and mean atmospheric temperature error. The relation between δT and $\delta\tau_6$ is linear for specific temperature and transmittance. On average, the LST error increases with transmittance error at the rate of 0.37°C for $\tau_6 = 0.8$ and 0.48°C for $\tau_6 = 0.7$. For mean atmospheric temperature, δT only depends on δT_a but does not change with T_a. The increase rate of δT with δT_a is determined by the ratio of parameter D_6 to C_6 (figure 7). Because the ratio is strongly affected by transmittance, the δT due to δT_a is also strongly related to transmittance. The higher the transmittance, the less the δT due to δT_a. For the ratio D6/C6 = 0.27 which corresponds to $\tau_6 = 0.8$, the probable δT is about 1°C for $\delta T_a = 3.5$°C. Therefore, high transmittance due to low water vapour in the atmospheric profile is the best condition for an accurate LST retrieval from Landsat TM6 data. When transmittance is above 0.8, the comprehensive LST error due to a moderate error in emissivity, transmittance and mean atmospheric temperature estimation is about 1.0–1.5°C.

The validation of the algorithm has been done to the various simulated situations for seven typical atmospheres. Using the atmospheric simulation program LOWTRAN 7.0, we simulate the thermal radiance at the satellite level and then use the radiance to convert into brightness temperature of TM6 for LST retrieval. Validation results indicate that the algorithm is able to provide a quite accurate LST estimate from TM6 data. The LST difference between the assumed and the retrieved ones is less than 0.4°C for most situations.

The algorithm has been applied to the Israel–Egypt border region as an example for analysing the spatial distribution of LST difference on both sides from the Landsat TM image taken on 29 March, 1995. Based on the available measurement of water vapour content and air temperature, we estimate the transmittance and mean atmospheric temperature for the retrieval. The result shown in figure 8 supports the observed surface temperature difference across the border in remote sensing imagery. The Israeli side does have obviously higher LST than the Egyptian side. This is because the biogenic crust that covers most of the ground surface on the Israeli side has much higher surface temperature than the bare sand prevailing on the Egyptian side (figure 9). Furthermore, the contribution of higher LST from biogenic crust covering up to two-thirds of ground surface on the Israeli side overwhelms the weak cooling process from more desert vegetation cover. Comprehensive assessment indicates that the probable LST estimation error due to the possible error in estimating the critical parameters of the algorithm is less than 1.1°C in the image. This error is lower than the generally accepted level 1.5°C. Thus, it can be concluded that the estimated LST distribution in the image is very close to the true one.

Acknowledgments

The authors would like to express the thanks to the Jacob Blaustein International Center for Desert Research for providing the fellowship to Zhihao Qin to conduct his study at the Laboratory. We also would like to thank Simon M. Berkowics, administrator of The Arid Ecosystem Research Center (AERC), Hebrew University of Jerusalem for his allowance to perform the ground truth measurement of this study in the Nizzana research site of AERC on the Israeli side of the border region.

References

Andres, R. J., and Rose, W. I., 1995, Description of thermal anomalies on two active Guatemalan volcanoes using Landsat Thematic Mapper imagery. *Photogrammetric Engineering and Remote Sensing*, **61**, 775–782.

Braga, C. Z. F., Setzer, A. W., and De Lacerda, L. D., 1993, Water quality assessment with simultaneous Landsat 5 TM data at Guanabara Bay, Rio de Janeiro, Brazil. *Remote Sensing of Environment*, **45**, 95–106.

Caselles, V., Artigao, M. M., Hurtado, E., Coll, C., and Brasa, A., 1998, Mapping actual evapotranspiration by combining Landsat TM and NOAA AVHRR images: Application to the barrax area, Albacete, Spain. *Remote Sensing of Environment*, **63**, 1–10.

Cole, A. E., Court, A., and Kantor, A. J., 1965, Model atmospheres. In *Handbook of Geophysics and Space Enviornments*, edited by S. L. Valley, Air Force (Cambridge:Cambridge Research Laboratories, Office of Aerospace Research, United States Air Force).

Coll, C., Caselles, V., Sobrino, A., and Valor, E., 1994, On the atmospheric dependence of the split-window equation for land surface temperature. *International Journal of Remote Sensing*, **15**, 105–122.

Cracknell, A. P., 1997, *The Advanced Very high Resolution Radiometer* (*AVHRR*) (London: Taylor & Francis).

França, G. B., and Cracknell, A. P., 1994, Retrieval of land and sea surface temperature using NOAA-11 AVHRR data in north-eastern Brazil. *International Journal of Remote Sensing*, **15**, 1695–1712.

Goetz, S. J., Halthore, R. N., Hall, F. G., and Markham, B. L., 1995, Surface temperature retrieval in a temperate grassland with multiresolution sensors. *Journal of Geophysical Research*, **100**, 25 397–25 410.

HAAKSTAAD, M., KOGELER, J. W., and DAHLE, S., 1994, Studies of sea surface temperatures in selected northern Norwegian fjords using Landsat TM data. *Polar Research*, **13**, 95–104.

HUMES, K. S., KUSTAS, W. P., MORAN, M. S., NICHOLS, W. D., and WELTZ, M. A., 1994, Variability of emissivity and surface temperature over a sparsely vegetated surface. *Water Resources Research*, **30**, 1299–1310.

HURTADO, E., VIDAL, A., and CASELLES, V., 1996, Comparison of two atmospheric correction methods for Landsat TM thermal band. *International Journal of Remote Sensing*, **17**, 237–247.

KANEKO, T., 1998, Thermal observation of the 1986 eruption of Izu Oshima Volcano (Japan) using Landsat TM data. *Advances in Space Research*, **21**, 517–520.

KANEKO, D., and HINO, M., 1996, Proposal and investigation of a method for estimating surface energy balance in regional forests using TM derived vegetation index and observatory routine data. *International Journal of Remote Sensing*, **17**, 1129–1148.

KARNIELI, A., 1997, Development and implementation of spectral crust index over dune sands. *International Journal of Remote Sensing*, **18**, 1207–1220.

KARNIELI, A., and TSOAR, H., 1995, Spectral reflectance of biogenic crust developed on desert dune sand along the Israel–Egypt border. *International Journal of Remote Sensing*, **16**, 369–374.

KERR, Y. H., LAGOUARDE, J. P., and IMBERNON, J., 1992, Accurate land surface temperature retrieval from AVHRR data with use of an improved split window algorithm. *Remote Sensing of Environment*, **41**, 197–209.

KIDRON, G. J., and YAIR, A., 1997, Rainfall-runoff relationship over encrusted dune surfaces, Nizzana, Western Negev, Israel. *Earth Surface Processes and Landforms*, **22**, 1169–1184.

KNEIZYS, F. X., SHETTLE, E. P., ABREU, L. W., ANDERSON, G. P., CHETWYND, J. H., GALLERY, W. O., SELBY, J. E. A., and CLOUGH, S. A., 1988, Users guide to LOWTRAN-7 Technical Report AFGL-TR-88-0177, Optical/Infrared Technology Division, US Air Force Geophysics Laboratory, Hascom Air Forace Base, Massachusetts.

LIU, G. R., and KUO, T. H., 1994, Improved atmospheric correction process in monitoring SST around the outfall of a nuclear power plant. *International Journal of Remote Sensing*, **15**, 2627–2636.

LI, Z. L., and BECKER, F., 1993, Feasibility of land surface temperature and emissivity determination from AVHRR data. *Remote Sensing of Environment*, **43**, 67–85.

LO, C. P., 1997, Application of Landsat TM data for quality of life assessment in an urban environment. *Computers Environment and Urban Systems*, **21**, 259–276.

MANSOR, S. B., CRACKNELL, A. P., SHILIN, B. V., and GORNYI, V. I., 1994, Monitoring of underground coal fires using thermal infrared data. *International Journal of Remote Sensing*, **15**, 1675–1685.

MARKHAM, B. L., and BARKER, J. L., 1986, Landsat-MSS and TM post calibration dynamic ranges, atmospheric reflectance and at-satellite temperature. *EOSAT Landsat Technical Notes 1*, (Lanham, Maryland: Earth Observation Satellite Company), pp. 3–8.

MCMILLIN, L. M., 1975, Estimation of sea surface temperatures from two infrared window measurements with different absorption. *Journal of Geophysical Research*, **36**, 5113–5117.

MORAN, M. S., JACKSON, R. D., RAYMOND, L. H., GAY, L. W., and SLATER, P. N., 1989, Mapping surface energy balance components by combining Landsat Thematic Mapper and ground based meteorological data. *Remote Sensing of Environment*, **30**, 77–87.

OPPENHEIMER, C., 1997, Remote sensing of the color and temperature of volcanic lakes. *International Journal of Remote Sensing*, **18**, 5–37.

PRATA, A. J., 1993, Land surface temperature from the advanced very high resolution radiometer and the along-track scanning radiometer. 1. Theory. *Journal of Geographical Research*, **98**, 16 689–16 702.

PRICE, J. C., 1984, Land surface temperature measurements from the split window channels of the NOAA 7 Advanced Very High Resolution Radiometer. *Journal of Geophysical Research*, 89**, 7231–7237.**

REDDY, C. S. S., BHATTACHARYA, A., and SRIVASTAV, S. K., 1993, Night time TM short wavelength infrared data analysis of Barren Island volcano, South Andaman, India. *International Journal of Remote Sensing*, **14**, 783–787.

Ritchie, J. C., Cooper, C. M., and Schiebe, F. R., 1990, The relationship of MSS and TM digital data with suspended sediments, chlorophyll, and temperature in Moon Lake, Mississippi. *Remote Sensing of Environment*, **33**, 137–148.

Saraf, A. K., Prakash, A., Sengupta, S., and Gupta, R. P., 1995, Landsat TM data for estimating ground temperature and depth of subsurface coal fire in the Jharia coalfield, India. *International Journal of Remote Sensing*, **16**, 2111–2124.

Schneider, K., and Mauser, W., 1996, Processing and accuracy of Landsat Thematic Mapper data for lake surface temperature measurement. *International Journal of Remote Sensing*, **17**, 2027–2041.

Schott, J. R., and Volchok, W. J., 1985, Thematic Mapper thermal infrared calibration. *Photogrammetric Engineering and Remote Sensing*, **51**, 1351–1357.

Singh, S. M., 1988, Brightness temperature algorithms for Landsat Thematic Mapper Data. *Remote Sensing of Environment,* **24**, 509–512.

Sobrino, J. A., Coll, C., and Caselles, V., 1991, Atmospheric correction for land surface temperature using NOAA-11 AVHRR channels 4 and 5. *Remote Sensing of Environment*, **38**, 19–34.

Sospedra, F., Caselles, V., and Valor, E., 1998, Effective wavenumber for thermal infrared bands application to Landsat TM. *International Journal of Remote Sensing*, **19**, 2105–2117.

Sugita, M., and Brutsaert, W., 1993, Comparison of land surface temperatures derived from satellite observations with ground truth during FIFE. *International Journal of Remote Sensing*, **14**, 1659–1676.

Sutherland, R. A., 1986, Broadband and spectral (2–18 μm) emissivity of some natural soils and vegetation. *Journal of Atmospheric and Oceanic Technology*, **3**, 199–202.

Takashima, T., and Masuda, K., 1987, Emissivities of quartz and Sahara dust powers in the infrared region (1–17 μm). *Remote Sensing of Environment*, **23**, 51–63.

Tsoar, H., and Karnieli, A., 1996, What determines the spectral reflectance of the Negev-Sinai sand dunes. *International Journal of Remote Sensing*, **17**, 3513–3525.

Tsoar, H., and Møller, J. T., 1986, The role of vegetation in the formation of linear sand dunes. In *Aeolian Geomorphology*, edited by W. G. Nickling (Boston: Allen and Unwin), pp.75–95.

Wukelic, G. E., Gibbons, D. E., Martucci, L. M., and Foote, H. P., 1989, Radiometric calibration of Landsat Thematic Mapper Thermal Band. *Remote Sensing of Environment*, **28**, 339–347.

Zhang, X., Van Genderen, J. L., and Kroonenberg, S. B., 1997, A method to evaluate the capability of Landsat 5 TM band 6 data for sub pixel coal fire detection. *International Journal of Remote Sensing*, **18**, 3279–3288.